High-resolution vehicle-based adaptive optical system with two-grade tip/tilt correction*

MING Ming (明名)[1,2], **CHEN Tao** (陈涛)[1,2]**, **and XU Tian-shuang** (徐天爽)[3]

1. Changchun Institute of Optics, Fine Mechanics and Physics, Chinese Academy of Sciences, Changchun 130033, China

2. University of Chinese Academy of Sciences, Beijing 100049, China

3. School of Mechanical and Aerospace Engineering, Jilin University, Changchun 130012, China

(Received 11 April 2018; Revised 29 May 2018)

The images obtained by a large optical detection system (>500 mm) are always blurred by atmospheric turbulence. To address this blurring, an adaptive optical system is urgently needed. Here, a 1.3 m vehicle-based adaptive optical system (VAOS), located on the Nasmyth focus, is investigated. A two-grade tip/tilt steering mirror is used to eliminate tracking jitter and atmospheric tipping error. Pupil matching and cooperation between the deformable mirror and the wavefront sensor are adopted to achieve high-order aberration measurement and correction via closed-loop correction and to allow the telescope to obtain high-quality imaging. For different seeing conditions and site locations, the VAOS achieves the sensing over the wavelength range from 0.5 μm to 0.7 μm using a Shack-Harmann wavefront sensor and the correction with a 97-unit deformable mirror for an imaging spectrum range from 0.7 μm to 0.9 μm. Moreover, the maximum detection capability of the system is greater than a visual magnitude of 5, and the angular imaging resolution is better than 0.3".

Document code: A **Article ID:** 1673-1905(2018)06-0411-6

DOI https://doi.org/10.1007/s11801-018-8055-4

With the development of large astronomical telescopes, adaptive optics is widely used. Hardy successfully developed the first adaptive optics system (AOS) and used the system to conduct real-time correction of horizontal atmospheric turbulence[1]. Now, the AOS of large binocular telescope makes use of a 672 actuator adaptive secondary mirror, also known as a deformable secondary mirror, which could yield diffraction-limited performance[2,3].

An AOS provides a practical approach for overcoming atmospheric turbulence. Specifically, wavefront sensors are used to measure wavefront phase distortion, and by closed-loop control, the wavefront corrector can correct the distorted wavefront in real time. When a planar wave passes through the atmosphere, it will be distorted by atmospheric turbulence[4,5]. The AOS can measure the wavefront distortion in real time using a wavefront sensor, and can realize imaging with diffraction-limited resolution capability via the wavefront corrector's real-time compensation. In 1975, a useful formula was presented for using Zernike polynomials to describe a wavefront[6,7].

At present, to ensure the stability of the optical systems, the AOS is designed through the Coude Optical Laboratory[8,13], which is located below the telescope tower. The AOS from Coude Laboratory can effectively improve the image resolution. And the 1.8 m telescope at Gaomeigu Observatory makes use of 127-element AOS to obtain resolution image with Coude system[14].

However, a telescope with a Coude AOS can observe only targets on a horizontal line, as shown in Fig.1. Because the earth is spherical, it is impossible to gain high-resolution images using a single telescope with the Coude AOS, leading to low observation efficiency.

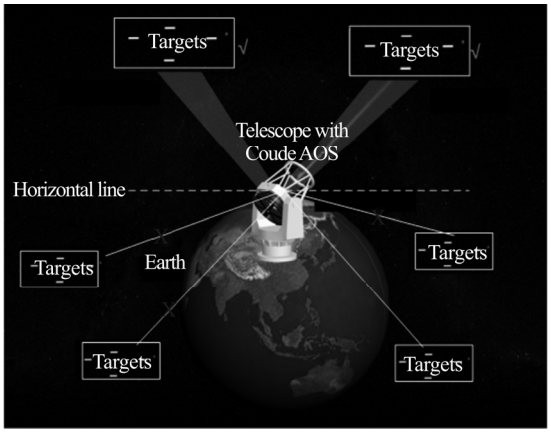

Fig.1 Observation limit of telescope with Coude AOS

In this paper, a method which uses a form of a vehicle-based adaptive optical system (VAOS) is proposed to obtain a high-resolution image, and the telescope with

* This paper has been supported by the National Natural Science Foundation of China (No.11703026).

** E-mail: 18643075226@163.com

the VAOS is movable, allowing observations of important targets at different longitudes and latitudes.

The VAOS is designed to simplify the construction and to realize high resolution under different atmospheric seeing conditions. As shown in Fig.2, based on a 1.3-m Nasmyth focal platform, an AOS is investigated. The AOS contains a two-grade tip/tilt corrector and a closed-loop system to remove the tilt caused by the atmosphere and survival tracking errors. The first grade corrects the tracking error, jitter and low-frequency tilt error of the atmospheric disturbances with the first fast-steering mirror (FFSM), and the second grade corrects the high-frequency tilt error of the atmospheric disturbances with the second fast-steering mirror (SFSM). The higher-order aberrations are corrected by a deformable mirror (DM).

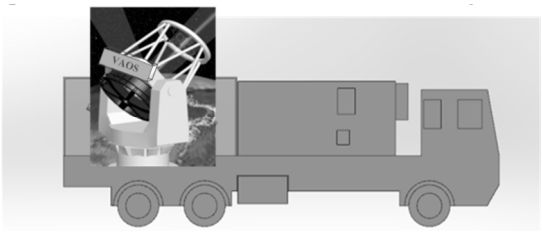

Fig.2 Vehicle telescope with a VAOS

In the VAOS, the tracking error, jitter and tip/tilt error of the atmosphere should be corrected. The tracking error and jitter are slow, changing at low frequency (≤200 Hz), whereas the tip/tilt error of the atmosphere is very fast, changing at frequencies higher than 1 000 Hz; thus, the system has two fast-steering mirrors (FSMs). The FFSM corrects the tracking error and parts of the tip/tilt error with low frequency, and the SFSM corrects all of the residual tip/tilt error with high frequency.

The VAOS consists of seven parts, which are the primary optics system, relay optics system, the first-order tip/tilt correction system, the second-order tip/tilt correction system, wavefront correction system and high-resolution imaging system. In this paper, we compare the imaging results of the optical system in practical applications. We find that the expected design results are in line with the imaging quality of the actual results, and the diffraction-limited resolution capability of the 1.3-m VAOS is achieved.

The primary optical system of the 1.3-m imaging system uses the form of the Nasmyth focus. As shown in Fig.3, a planar wave from infinity enters the telescope, is reflected by the primary and secondary mirrors, and is then guided by M3 into the Nasmyth focus, docking with the AOS[15,16].

The primary optical system in the form of the Nasmyth focus enables the collection of optical energy with a large aperture and beam transmission in the optical system, and provides a beam with a good wavefront in the field of view. Tab.1 presents the related parameters for the primary optical system.

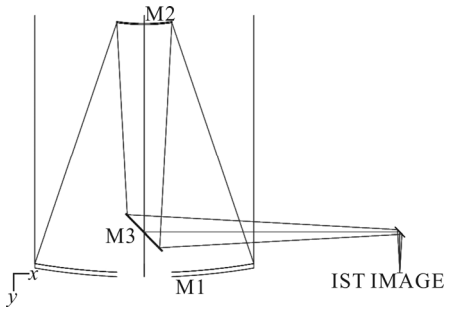

Fig.3 Optical layout of the Nasmyth focus system

Tab.1 Parameters for the primary optical system

Optical parameters	Required index
Aperture (mm)	1.3 m
Focal length	18 m
Field of view	5′
Obscuring ratio	<5%
Spectral range	0.5—1.7 μm

The AOS is located on the vehicle-based Nasmyth focus platform of the 1.3-m telescope. The focused beam reflected by the planar M3 is collimated by the relay optical system and then successively guided into the tilt correction system, wavefront sensing system and high-resolution imaging system by the spectrum system. The optical layout is shown in Fig.4.

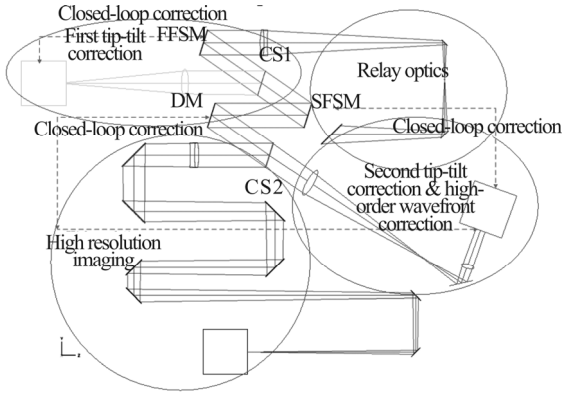

Fig.4 Optical layout of the VAOS

The relay optical system collimates the focused beam of the primary optical system into a parallel beam and provides an exit pupil for the system, which is located in the middle of the tip-tilt mirror. Furthermore, the wavefront error is used to evaluate the imaging quality of the relay optical system. CS1, as the key component of the spectrum, reflects a part of the visible beam (0.4—0.5 μm) into the first tilt correction system, and the remaining part of the visible beam and the near-infrared beam (0.5—0.9 μm) are separated by CS2. The visible beam (0.5—0.7 μm) is transmitted into a second tilt correction system and wavefront detection system, and the near-infrared beam (0.7—0.9 μm) is reflected into the high-resolution imaging system. As shown in Fig.4, the VAOS is integrated on a platform of a certain size to realize two-grade tilt correction,

adaptive correction and high-resolution imaging with beams at different wavelengths.

The design of an AOS should consider conjugation of all pupils for the system. The DM and Shack-Hartmann wavefront sensor should be conjugated with the entrance pupil of the system. Thus, the FFSM and the SFSM should be placed near the DM to avoid pupil movement.

The influence of atmospheric turbulence on the imaging quality of the telescope is classified into two categories of global tilt of the wavefront and partial wavefront distortion.

According to the Kolmogorov atmospheric turbulence theory[7], the wavefront root mean square (RMS) tilt at the pupil can be expressed as

$$\sigma_{\text{uncomp}}=\sqrt{0.182\cdot(D/r_0)^{5/3}\cdot(\lambda/D)^2}\ \text{rad}. \quad (1)$$

The 2.5-fold standard deviation of the normal distribution can cover a range of approximately 98.4%. For the telescope, D=1.3m, λ=500nm, r_0=7 cm, and the corresponding global tilt can be expressed as $\Delta_{\text{tt}}=\pm2.5\sigma_{\text{uncomp}}=\pm2.7''$.

In addition to the global tilt of the wavefront, the system also exhibits the residual tracking error, which directly influences the wavefront tilt of the entrance pupil. Moreover, the wavefront tilt of the 1.3-m telescope caused by the residual tracking error Δ' is less than 5". Thus, the global wavefront tilt to be corrected at the entrance pupil of the telescope is

$$\delta=\pm\sqrt{\Delta_{\text{tt}}^2+\Delta'^2}=\pm5.7''. \quad (2)$$

The tilt detection and correction system primarily performs two functions. One function is to measure and correct the global tilt of the wavefront, and the other function is to measure and correct the tilt of the wavefront caused by the residual tracking error of the system.

According to the object-image relationship, the magnification m is determined by the entrance pupil and tip/tilt mirror, that is, m=1 300/40=32.5. Thus, the stroke of the tip/tilt mirror is $\delta'=32.5\delta=3.1'$. The optical parameters of the tilt detection and correction system can be obtained by calculation: the pixel resolution is between 0.5" and 1", the operating wavelength range is from 0.4 μm to 0.5 μm, the field of view is 2′, and the stroke of the tilt mirror is greater than ±3′. Tab.2 shows the parameters of the tip-tilt mirror. With the help of spectroscopy, the tilt detection correction system realizes detection and correction of the global tilt of the wavefront at the entrance pupil in the wavelength range of 0.4—0.5 μm.

Tab.2 Parameters of the tip-tilt mirror

	FFSM	*SFFM*
Component type	Flat mirror	Flat mirror
Surface accuracy	10 nm (*RMS*)	10 nm (*RMS*)
Resonant frequency	200 Hz	1 000 Hz
Stroke	±300"	±60"
Clear aperture	76 mm	76 mm

According to the exposure time and quantum efficiency of sensor (Andor du860), the sample frequency of the first closed-loop system is lower than 200 Hz, and the bandwidth is less than 40 Hz. The corrected precision of the FFSM closed-loop system is better than 0.3".

Fig.4 shows the combined layout of the second tilt correction system and the wavefront correction system, and Tab.2 gives the basic parameters of the SFSM.

The second tilt closed loop uses the wavefront detector to measure the residual tip/tilt errors, which may contain jitter from the telescope and major atmospheric slope.

The feedback component uses the Shack-Hartmann wavefront sensor to measure the global slope, which adopts the Zernike fringe polynomial model. To eliminate all other tip/tilt errors, the frequency is much higher than that of the FFSM closed-loop system. Based on the sampling frequency of the Shack-Hartmann sensor, the sample frequency of the second closed-loop system is higher than 1 000 Hz, and the bandwidth is higher than 100 Hz. With the high-frequency correction, the precision of the FFSM closed-loop system is better than 0.1".

Tab.3 shows the basic parameters of the wavefront sensing system. The closed loop is composed of a Shack-Hartmann wavefront sensor (S-H) and a DM. The wavefront sensor measures the high-order distortion caused by atmospheric turbulence and residual static aberration of the system, while the DM performs real-time correction.

Tab.3 Parameters of the wavefront sensing system

Parameter	Value
Units of the DM	97
Aperture of the DM	76 mm
Subaperture size of S-H	200 μm (0.1 m on M1)
Single aperture FOV of S-H	10″×10″
Single aperture pixels of S-H	10 pixel×10 pixel
Wavefront processor architecture	FPGA+DSP

A 97-unit discrete piezoelectric DM with a continuous surface shape was used, where 97 units are used, and the piezoelectric actuator is arranged in an 11×11 square. The correction stroke of the actuator is greater than ±2.5 μm, and the mechanical resonance frequency is higher than 12 kHz. The microlens array of the wavefront detectors is also arranged in a square shape, and the microlenses and the DM actuators correspond, one by one, to each other using a Southwell model map[17]. The wavefront processor in the system realizes high-speed wavefront detection processing and wavefront correction control based on a field-programmable gate array (FPGA) and a digital signal processor (DSP). The wavefront processor includes a single-board computer, a wavefront-processing board and an expandable wavefront-processing board. Among them, the single-board computer primarily performs non-real-time manipulation and management functioning. The wavefront-processing board based on an FPGA mainly achieves real-time wavefront detection processing, and the wavefront-processing subboard completes the real-time wavefront correction control. The experimental results show that

the total delay of the wavefront processing is approximately 62 ms, which is much less than the output time of the wavefront detector images.

The imaging system is the last terminal of the VAOS. After the wavefront correction and the correction of the system, the light beams entering the imaging system achieve imaging at the diffraction limit.

The VAOS uses DV887 as the image detector, and the single pixel dimension (ρ) is 16 μm. According to the Nyquist sampling theorem, the focal length is

$$f=\frac{2\rho}{1.22\lambda}\times D=\frac{2\times 16}{1.22\times 0.8}\times 1.3=42.63\ \text{m}\ . \tag{3}$$

And the resolution of the optical system near the diffraction limit is expressed by the full width half maximum (*FWHM*). The RMS of the wave aberrations of the system in the full field of view is less than $\lambda/43$, when λ=0.8 μm. The point spread function curve of the high-resolution imaging system is based on the evaluation criterion of the *FWHM*. This curve reflects the resolution of the system for imaging the space target, and the *FWHM* of the system in the full field of view is less than 0.135".

Fig.5 presents a wavefront aberration test pattern of the adaptive detection and correction system with a relay optical system, a DM and a wavefront sensing system. The data show that the wavefront aberration of the whole detection and correction system, including the DM fitting error, Shack-Hartmann wavefront measuring error and controlling wavefront fitting error, can reach $\lambda/60$ (λ=632.8 nm) after the DM is flattened.

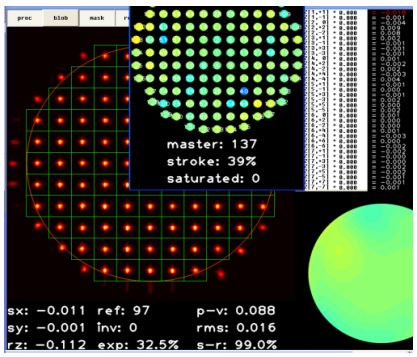

Fig.5 Wavefront test pattern

Dynamic testing provides a corrective evaluation for tilt disturbances and high-order disturbances. In the test, based on phase screen simulations of different atmospheric conditions, we obtain the closed-loop tracking accuracy, the error suppression bandwidth and the imaging Strehl ratio (*SR*), which is used as an evaluation index. For r_0=7 cm, the relationship between the measured *SR*, disturbance Greenwood frequency f_G and S-H sensor signal-to-noise ratio (*SNR*) is shown in Fig.6.

In the higher-order distortion correction test, the frame rate of the DU860 camera used in the wavefront detector is 500 Hz, and the light source brightness is adjusted based on the Greenwood frequency f_G and r_0. Here, r_0 is the atmospheric coherence length, which is given by $\delta_{seeing}=1.22(\lambda/r_0)$, where δ_{seeing} is the diffraction limit. Moreover, r_0 value simulated by the phase screen is set as 7 cm for the wavelength of 632.8 nm. Based on the image *SNR* of different wavefront sensors, the adaptive system corrects tilting and high-order distortion and collects images from an imaging camera. Moreover, the imaging *SR* is used to test the correction capability of the adaptive system.

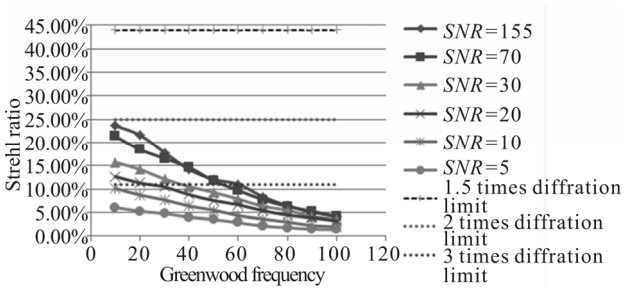

Fig.6 Correction performance of AOS when r_0=7 cm

Fig.7 shows experimental images obtained by the high-resolution imaging camera of the adaptive system before and after correction, where the atmospheric turbulence is modulated as *SNR*=30, r_0=7 cm and f_G=60 Hz. As shown in Fig.7, the adaptive system achieves an excellent correction effect, which is achieving diffraction-limited.

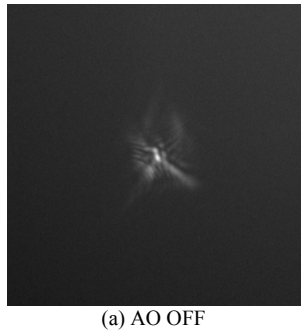

(a) AO OFF

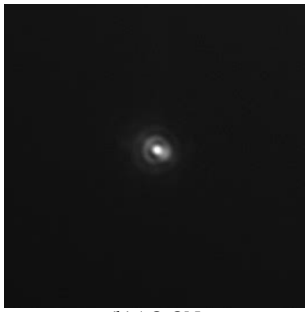

(b)AO ON

Fig.7 Experimental imaging of the AOS with *SNR*=30, r_0=7 cm and f_G=60 Hz

The measured average r_0 of the site is 9 cm. Fig.8 shows a 5.03-magnitude star comparison graph of the wavefront aberration at the exit pupil of the system measured by the wavefront sensor before and after adaptive correction, and the imaging comparison. The static aberration of the atmospheric turbulence fusion system is 0.637λ before the adaptive optical correction

and 0.081λ (close to the diffraction limit) after adaptive optical correction.

Fig.8 shows an imaging comparison for a 5.03-magnitude star before and after the adaptive correction. After correction, the imaging resolution of the system for the fixed star is 0.3" (twice of the diffraction limit). Correspondingly, Fig.9 shows a double star imaging comparison for 5.28-magnitude and 5.39-magnitude stars before and after adaptive correction. The imaging resolution of the high-resolution imaging system for the double star is 0.35" (nearly twice of the diffraction limit).

Based on the results of star correction and observation imaging in the AOS, several features of the VAOS can be obtained. First, the DM is completely conjugated with the entrance pupil of the system, and the FFSM and SFSM are near the DM, which reduces the number of required relay optical components and effectively improves the optical efficiency.

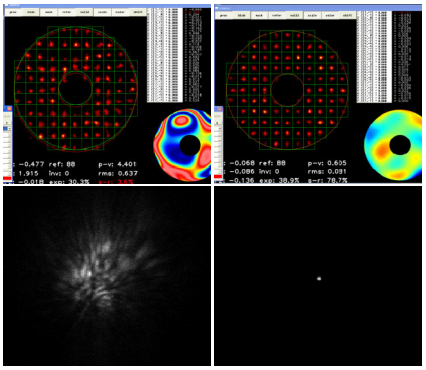

Fig.7 Single-star comparison of the wavefront and image before and after correction with r_0=9 cm

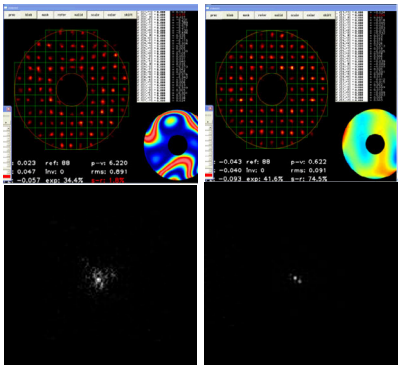

Fig.8 Double-star comparison of the wavefront and image before and after correction with r_0=6 cm

Furthermore, the compact structure can resolve spatial problems in the AOS. Thus, the AOS can realize high-resolution imaging at different sites and under different atmospheric seeing conditions. Moreover, the primary optical system and the VAOS are independent, and the configuration detection of two systems can be independently implemented. Furthermore, the VAOS can realize the transformation of adaptive optics from stationary to mobile without eliminating imaging rotation.

The traditional Coude AOS is unable to observe space targets at sites with different atmospheric seeing conditions. To address this issue, a novel VAOS is designed in this paper, which has several advantages compared with Coude AOS. The focal point of a Nasmyth focus is used as the docking platform of the VAOS, and a relay optical system is used to achieve complete matching for the entrance pupil, FFSM, SFSM and DM. To achieve high-quality imaging, the primary optical system takes the form of a Cassegrain system, with the VAOS on the telescope platform. In this paper, the imaging results at different sites and for different seeing observations are better than a visual magrutude of 5, and the resolution of the system is 0.3" (twice of the diffraction limit).

References

[1] Hardy J. W, Adaptive Optics for Astronomical Telescopes, Oxford Univ. Press, (1998).

[2] J. C. Christou, G. Brusa, A. Conrad, S. Esposito, T. Herbst, P. Hin, J. Hill, D. Miller, S. Rabien, G. Rahmer, G. Taylor, C. Veillet and X. Zhang, Adaptive Optics Capabilities at the Large Binocular Telescope Observatory, Proc. of SPIE **9909**, 99092E-1 (2016).

[3] G. Brusa, D. Ashby, J. C. Christou, J. Kern, M. Lefebvre, T. J. Mcmahon, D. Miller, G.Rahmer, R. Sosa, G. Taylor, C. Vogel and X. Zhang, Engineering Aspects of the Large Binocular Telescope Observatory Adaptive Optics Systems, Proc. of SPIE **9909**, 990903-1 (2016).

[4] Donald Gavel, Renate Kupke, Alexander R.Rudy, Srikar Srinath, Daren Dillon and Lisa Poyneer, Lick Observatory's shane telescope adaptive optics system (ShaneAO): research derections and progress, Proc. of SPIE **9909**, 99092W-1 (2016).

[5] Jun Ho Lee, Sunmy Shin, Gyu Nam Park, Hyug-Gyo Rhee and Ho-Soon Yang, Current Optics and Photonics **1**, 107 (2017).

[6] Tyson R. K, Adaptive Optics Engineering Handbook, (2000).

[7] Fried D J, Theoretical Study of Nonstandard Imaging Concepts, RADC-TR, 74-185 (1974).

[8] Michael Goodwin, Jessica Zheng, Jon Lawrence, Samuel Richards, Alexander Arriola, Nick Cvetojevic, Simon Gross and Barnaby Norris. Adaptive optics on-sky demonstrator for the Anglo-Australian Telescopem, Proc. of SPIE **9909**, 990933-1 (2016).

[9] B. Maritz, M. S. Koago, C. K. Wainman, M. E. Gardener, W. H. Gunter and A. M. Eijk, Vertical Atmospheric Variability Measured Above Water During the FESTER Experiment: First Results, Optics in Atmospheric Propagation and Adaptive Systems XIX, 2016100020B (2016).

[10] Zhao Yong-chuang, Nie Zhong-quan, Zhai Ai-ping, Tian Yan-ting, Liu Chao, Shi Chang-kun and Jia Bao-hua, Optoelectronics Letters **14**, 21 (2018).

[11] E. Kopylov, L. Bolbasova, N. Goleneva, V. Lavrinov and A. Yu Shikhovtsev, Investigations of Parameters of Image Quality for Adaptive Optical Systems of BSVT, Proc. of SPIE **9680**, 96801O-1 (2015).

[12] Ju G., Yan C., Gu Z. and Ma H, Optics Express **24**, 24665 (2016).

[13] Changhui Rao, Kai Wei, Lei Zhu, Xuejun Zhang, Xuejun Rao, Shengqian Wang, Xiaoyu Ma, Lanqiang Zhang, Youming Guo, Ang Zhang, Hua Bao, Luchun Zhou, Mei Li, Chunlin Guan, Xiaojun Zhang, Xinlong Fan, Donghong Chen, Hao Xian, Yudong Zhang and Wenhan Jiang, Astronomical AO in Key Laboratory of Adaptive Optics, Chinese Academy of Sciences, Proc. of SPIE 9909, 990919-1(2016).

[14] Mark Chun, Olivier Lai, Douglas Toomey, Jessica Lu, Max Service, Christoph Baranec, Simon Thibault, Denis Brousseau, Yutaka Hayano, Shin Oya, Shane Santi, Christopher Kengery, Keith Loss, John Gardiner and Brad Steele, Imaka - a Ground-Layer Adapt ive Optics System on Maunakea, Proc. of SPIE **9909**, 990902-1 (2016).

[15] Chelo Ferreira, Jose L. Lopez, Rafael Navarro and Ester Simusia, Applied Optics **54**, 6575 (2015).

[16] Zhang Feng and Zhong Jin-gang, Optoelectronics Letters **2**, 31 (2006).

[17] Laurent Jolissaint, Onur Keskin, Lorenzo Zago, Sinan Kaan Yerli, Cahit Yesilyaprak Mudry and Gregory Lousberg, The Design of an Adaptive Optics Telescope: the Case of DAG, Proc. of SPIE **9906**, 99063J-1 (2016).